ACS Photonics

Article

Cite This: ACS Photonics 2018, 5, 3263−3271

Enhancing Upconversion Luminescence Emission of Rare Earth Nanophosphors in Aqueous Solution with Thousands Fold Enhancement Factor by Low Refractive Index Resonant Waveguide Grating

Duc Tu Vu,[†] Hsien-Wen Chiu,[†] Robasa Nababan,[†] Quoc Minh Le,[‡,§] Shiao-Wei Kuo,[∥] Lai-Kwan Chau,[⊥] Chu-Chi Ting,[#] Hung-Chih Kan,[†] and Chia-Chen Hsu*[,†,#]

[†]Department of Physics, National Chung Cheng University, Ming Hsiung, Chia Yi, 621, Taiwan

[‡]Institute of Materials Science, VAST of Vietnam, Hoang Quoc Viet Road, Hanoi, 100000, Vietnam

[§]Duy Tan University, Quang Trung Road, Danang, 550000, Vietnam

[∥]Department of Materials and Optoelectronic Science, National Sun Yat Sen University, Kaohsiung, 804, Taiwan

[⊥]Department of Chemistry and Biochemistry, National Chung Cheng University, Ming Hsiung, Chia Yi, 621, Taiwan

[#]Graduate Institute of Opto-Mechatronics, National Chung Cheng University, Ming Hsiung, Chia Yi, 621, Taiwan

Supporting Information

ABSTRACT: The enhancement of upconversion luminescence (UCL) of rare earth doped upconversion nanoparticles (UCNPs) in aqueous solution is particularly important and urgently required for a broad range of biomedical applications. Herein, an effective approach to achieve highly enhanced UCL from $NaYF_4$:Yb^{3+},Tm^{3+} UCNPs in aqueous solution is presented. We demonstrate that UCL of these UCNPs can be enhanced more than 10^4-fold by using a mesoporous silica low refractive index resonant waveguide grating (low-n RWG) in contact with aqueous solution, which makes it well-suited for biomedical applications. The structure parameters of the low-n RWG are tuned via rigorous coupled-wave analysis simulation to ensure strong local excitation field to form atop the TiO_2 surface of the low-n RWG, where UCNPs are deposited. As the low-n RWG is excited by a near-infrared laser at 976 nm to match its guided mode resonance (GMR) condition, UCL emitted from UCNPs is greatly enhanced thanks to the strong interaction between excitation local field and UCNPs. UCL emission of UCNPs can be further enhanced about two to four times when the UCL emission condition (wavelength and angle) matches with the GMR condition. Furthermore, we show that the presence of biotin molecules atop of the low-n RWG can be easily detected through UCL emission generated from streptavidin-functionalized UCNPs with the help of the streptavidin−biotin specific binding. The results indicate that the low-n RWG has high potential for UCL biosensing and bioimaging applications.

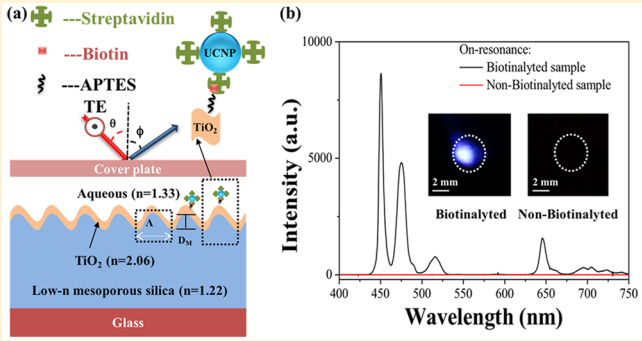

KEYWORDS: *guided mode resonance, low refractive index material, resonant waveguide grating, upconversion luminescence, upconversion nanoparticles*

Rare earth (RE) ions doped upconversion nanoparticles (UCNPs) have attracted great attention over the past decade due to their unique upconversion luminescence (UCL) properties. UCNPs can be excited by near-infrared (NIR) light and emit ultraviolet−visible luminescence with higher photon energy through a multiphoton absorption process.[1−3] UCNPs are particularly suitable to be used as photonic biomarkers in bioimaging and biosensing applications[4−6] because they do not have the problems like photobleaching and autofluorescence that most traditional fluorophores encounter. In addition, UCNPs can provide advantages such as good photostability, low scattering, no blinking, high signal-to-noise ratio, sharp emission line, large anti-Stokes shifts, long luminescence lifetimes, deep penetration in tissue, biocompatibility, low toxicity, and water solubility.[1−3] Various types of highly efficient UCNPs have been developed; with a typical one comprises sodium yttrium fluoride ($NaYF_4$) host codoped with ytterbium (Yb^{3+}) sensitizer ions and activator ions, for example, erbium (Er^{3+}), thulium (Tm^{3+}), or holmium (Ho^{3+}).[7−9] However, up to now, UCL quantum yields of RE ions doped UCNPs are rather low,[10] especially in aqueous solution, which limits them

Received: April 16, 2018
Published: May 14, 2018

DOI: 10.1021/acsphotonics.8b00494
ACS Photonics 2018, 5, 3263−3271

to be widely used in bioimaging and biosensing applications. One of the greatest trends and major challenges in the field of UCNPs research is the quest to enhance UCL efficiency. Different approaches have been employed to enhance UCL efficiency of RE ions doped UCNPs, including material improvements,[11−15] photonic crystal effect,[16,17] plasmonic effect,[18−22] and guided mode resonance (GMR) effect.[23] Among them, GMR effect produced from a resonant waveguide grating (RWG) structure is the most promising method because it has yielded the highest enhancement factor of UCL of UCNPs, that is, 10^4-fold.[23]

The RWG is a multilayer structure containing a high refractive index covering layer (e.g., titanium dioxide (TiO_2)) deposited on the top of a low refractive index waveguide grating layer (e.g., SU-8). Strong local field can be built on the top surface of the covering layer if the RWG is excited under resonant excitation configuration; that is, the incident angle and wavelength of the excitation light simultaneously matching with the resonant angle and wavelength of a guided-mode of the RWG.[24,25] The RWGs are widely used for enhancing light−matter interaction[26−28] and are especially powerful for increasing nonlinear light−matter interaction, for example, two-photon fluorescence,[27] second harmonic generation,[28] and UCL.[23] Previously, we demonstrated that UCL from a UCNPs-doped poly(methyl methacrylate) (PMMA) thin film deposited on top of a RWG containing a SU-8 waveguide grating layer, hereafter referred to as the SU-8 RWG, can be greatly enhanced by the GMR effect under resonant excitation configuration.[23] However, in that study, UCNPs were immersed in the PMMA polymer matrix, not in an aqueous environment. To be eligible for bioimaging and biosensing applications, the PMMA thin film has to be replaced by aqueous solution. Unfortunately, this will move the strong local field away from the top surface of the TiO_2 covering layer, where UCNPs will be deposited, to the inner region of the SU-8 waveguide grating layer due to SU-8 possessing higher refractive index than aqueous solution. Consequently, the SU-8 RWG is not suitable for enhancing UCL of UCNPs in aqueous environment. To build a strong local field on the top surface of the TiO_2 covering layer, a material with refractive index smaller than that of aqueous solution should be used in the waveguide grating layer to form a reverse symmetry waveguide structure.[29−31]

Herein, a low refractive index (low-n) RWG, made up of a low-n mesoporous silica waveguide grating layer, is presented to produce strong local field on its top surface, on which UCNPs are deposited and covered with aqueous solution. We demonstrate that UCL of UCNPs in aqueous solution is enhanced more than 10^4 fold under resonant excitation configuration. To further evaluate the feasibility of using the combination of UCNPs and low-n RWG for UCL biosensing and bioimaging applications, top surface of the TiO_2 covering layer of the low-n RWG is immobilized with biotin. Strong UCL is generated after drop-casting of streptavidin-conjugated UCNPs (UCNPs-SA) on the biotinylated TiO_2 surface thanks to the specific binding between streptavidin and biotin moieties. The result confirms that the low-n RWG can be used as a platform for UCL biosensing and bioimaging applications.

RESULTS AND DISCUSSION

The rigorous coupled-wave analysis (RCWA) simulation was used to find an appropriate design of the RWG structure to produce strong local field on its top surface. A one-dimensional sinusoidal RWG was considered and it contains, from top to bottom, a cover plate, an aqueous solution layer, a TiO_2 covering layer, a waveguide grating layer composed of either SU-8 photoresist or mesoporous silica, and a glass substrate. In the simulation, the following parameters were used. The thickness of the TiO_2 covering layer (T_{TiO2}) is 60 nm. The period (Λ) and the modulation depth (D_M) of the grating on the waveguide grating layer are 680 and 130 nm, respectively, and the thickness of the waveguide grating layer (T_{WG}) is 1.9 μm. The refractive indices of materials at 976 nm wavelength used in the RWG are as follows: cover plate $n_{cover\ plate}$ = 1.51, aqueous solution n_{aq} = 1.33, TiO_2 n_{TiO2} = 2.06, mesoporous silica $n_{mp\text{-}silica}$ = 1.22 (determined from ellipsometry measurement), SU-8 $n_{SU\text{-}8}$ = 1.55, and glass n_{glass} = 1.51. Figure 1a displays the calculated electric field intensity ($|E|^2$) distribution (normalized to the unit amplitude of the incident field) in the SU-8 RWG flooded with aqueous solution for the transverse electric (TE) GMR mode obtained with the incident wavelength (λ) at 976 nm ($NaYF_4$:Yb^{3+},Tm^{3+} UCNPs have absorption at 976 nm) and the incident angle (θ) at 4.25°. It is clear to observe that the maximum of the electric field intensity is highly localized inside the SU-8 waveguide grating layer. In contrast, as shown in Figure 1b, when the low-n RWG is illuminated by a collimated light at 976 nm with θ = 2.75°, the maximum of the electric field intensity is shifted upward to the TiO_2 covering layer thanks to the reverse symmetry waveguide structure design ($n_{mp\text{-}silica} < n_{aq}$).[29−31] By using a program written in MATLAB, the average values of $|E|^2$ ($\langle|E|^2\rangle$) of SU-8 and low-n RWGs in a unit cell volume within a distance of 100 nm to the TiO_2 surface were found to be 50 and 95, respectively. It is clear that the low-n RWG is more suitable for enhancing UCL of UCNPs in aqueous solution.

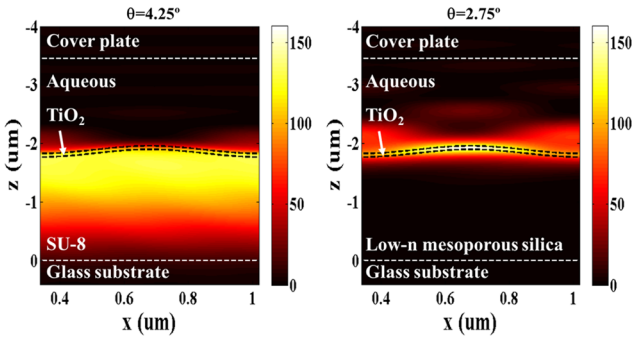

Figure 1. Calculated TE mode electric-field intensities ($|E|^2$) in the RWG under resonant excitation condition: (a) SU-8 RWG covered with aqueous solution; (b) Low-n RWG covered with aqueous solution.

The RCWA simulation was further employed to find a proper structure design of the low-n RWG to produce strong local electric field atop of the TiO_2 covering layer under resonant excitation configuration. Besides the index of refraction of the waveguide grating layer, other structural parameters such as thickness and period of the waveguide grating layer and thickness of TiO_2 covering layer also affect the electric field distribution in the low-n RWG structure. We first investigated the effect of the thickness of the waveguide grating layer on the $\langle|E|^2\rangle$ value by varying T_{WG} from 0.5 to 4.5 μm, and fixing T_{TiO2} = 60 nm, Λ = 700 nm, and D_M = 130 nm. The calculation result (see Figure 2a) shows that the $\langle|E|^2\rangle$ value increases with T_{WG} and the $\langle|E|^2\rangle$ value reaches to maximum

DOI: 10.1021/acsphotonics.8b00494
ACS Photonics 2018, 5, 3263−3271

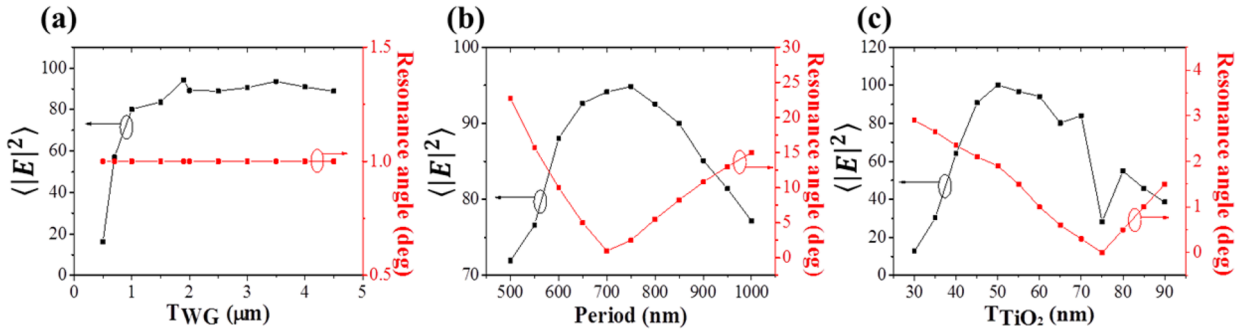

Figure 2. Calculated $\langle |E|^2 \rangle$ value and resonance angle versus (a) the thickness of the waveguide grating layer (low-n mesoporous silica), (b) the grating period, and (c) the thickness of TiO_2.

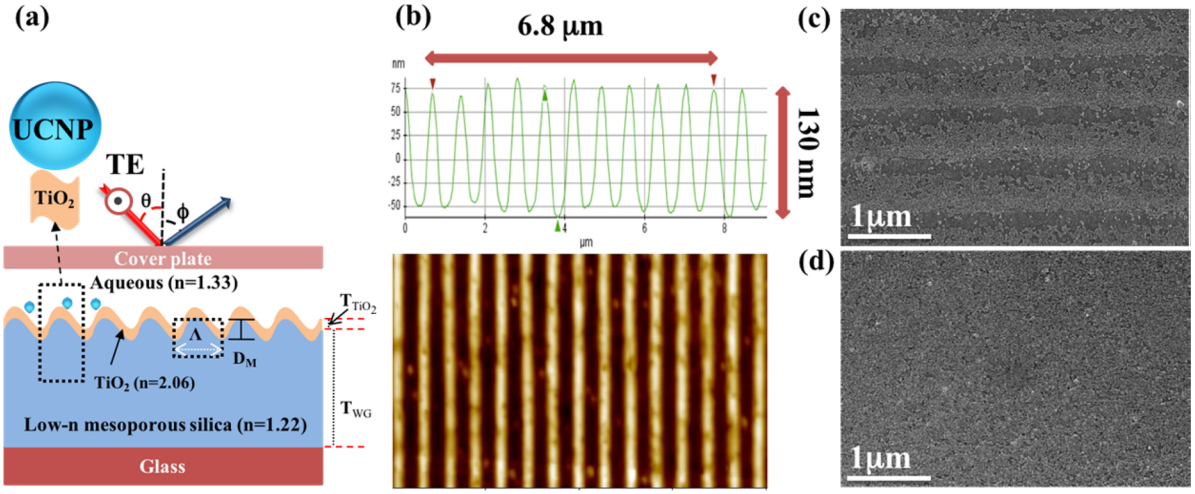

Figure 3. (a) Schematic of the low-n RWG sample. Its top surface was first deposited with UCNPs by dip-coating method, then covered with aqueous solution. θ and ϕ are the excitation beam incident angle and the UCL detection angle relative to the surface normal direction, respectively. (b) AFM image of the surface morphology of the TiO_2 layer, the arrows represent the distance of ten grating periods and the modulation depth of the low-n RWG. (c) FESEM image of the low-n RWG after the deposition of UCNPs. (d) FESEM image of nongrating area covered with UCNPs.

and saturates for $T_{WG} \geq 1.9$ μm. The calculation also shows that the excitation resonance angle remains unchanged at 1° with the variation of T_{WG}. Figure 2b shows the dependence of the $\langle |E|^2 \rangle$ value and the resonance angle for resonant excitation condition on Λ, with $T_{WG} = 1.9$ μm, $T_{TiO2} = 60$ nm, and $D_M = 130$ nm. The calculation result shows that the low-n RWG with $\Lambda \approx 700-750$ nm can produce the highest $\langle |E|^2 \rangle$ value with the resonant incident angle around 1°. Herein, Λ around 700 nm was chosen as the period of the low-n RWG. Finally, the effect of the thickness of the TiO_2 covering layer was studied. Figure 2c shows the $\langle |E|^2 \rangle$ value as a function of the thickness of the TiO_2 covering layer and resonance angle obtained by assuming $T_{WG} = 1.9$ μm, $\Lambda = 700$ nm, and $D_M = 130$ nm. The calculation result indicates that the optimized thickness of the TiO_2 covering layer is around 50−60 nm and its resonance angle is between 1° and 2°. According to the simulation results, the structure parameters $T_{WG} = 1.9$ μm, $\Lambda = 700$ nm, $T_{TiO2} = 60$ nm, and $D_M = 130$ nm were chosen as the guideline for the fabrication of the low-n RWG.

Figure 3a shows the schematic diagram of the low-n RWG structure fabricated in this work, whose structural parameters were chosen based on the RCWA simulation result. Figure 3b displays the atomic force microscopy (AFM) image of the surface morphology of the TiO_2 layer which confirms the period and the modulation depth of the low-n RWG are 680 and 130 nm, respectively, close to those of the design structure.

In addition, we also confirmed $T_{WG} = 1.9$ μm with an α-step and $T_{TiO2} = 60$ nm with AFM measurements. To produce highly efficient UCL, monodisperse $NaYF_4$:Yb^{3+},Tm^{3+} UCNPs were deposited atop of the low-n RWG. Figure 3c shows the field emission scanning electron microscope (FESEM) image of the low-n RWG after the deposition of UCNPs. It clearly displays that UCNPs are mainly deposited atop of the low-n RWG, where the strong electric filed is localized. The nanoparticles are not uniformly deposited on RWG area due to the nature of nonflatting of the RWG structure. Figure 3d presents the distribution of UCNPs on non-RWG (nongrating) area. To characterize physical properties of UCNPs, transmission electron microscopy (TEM), X-ray diffraction (XRD), and UCL spectrum were taken. Figure S1a displays the TEM image of UCNPs, which reveals those particles have average diameter of 15 ± 3 nm. From the powder XRD analysis, we found that the synthesized UCNPs were pure β-phase and no diffraction peak associated with cubic phase of $NaYF_4$ crystals or NaF impurities were found (Figure S1b). Figure S1c displays the UCL spectrum of the $NaYF_4$:Yb^{3+},Tm^{3+} nanoparticles in cyclohexane, and it exhibits five emission bands centered around 450, 480, 645, 694, and 800 nm corresponding to the $^1D_2 \rightarrow {}^3F_4$, $^1G_4 \rightarrow {}^3H_6$, $^1G_4 \rightarrow {}^3F_4$, $^3F_3 \rightarrow {}^3H_6$, and $^3H_4 \rightarrow {}^3H_6$ transitions of thulium ions, respectively. The inset shows a photograph of the sample under NIR excitation.

DOI: 10.1021/acsphotonics.8b00494
ACS Photonics 2018, 5, 3263−3271

To find out the resonant excitation (GMR) condition of the UCNPs deposited low-n RWG sample (covered with aqueous solution), we calculated its TE mode transmission spectra at different incident angel θ. Figure 4a shows the calculation result

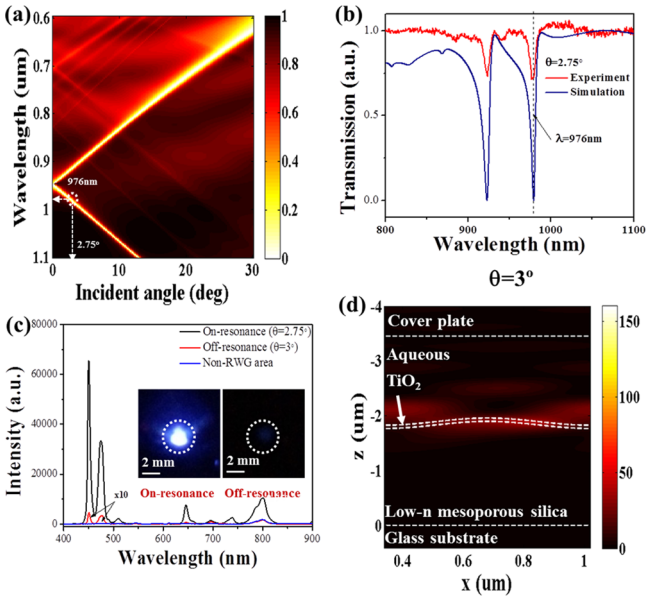

Figure 4. (a) Calculated transmittance in TE mode of the UCNPs deposited low-n RWG covered with aqueous solution as a function of incident angle and wavelength, the circle indicates the laser wavelength (976 nm) is matched with the GMR mode at the incident angle (θ = 2.75°). (b) Measured and calculated transmission spectra of the sample at the incident angle of 2.75°. (c) UCL spectra obtained from the RWG area of the sample under on-resonance (θ = 2.75°) and off-resonance (θ = 3.00°) and that obtained from the non-RWG area of the sample. Insets show optical images of the UCL emission of the sample taken with on-resonance and off-resonance excitation conditions. (d) Calculated TE mode $|E|^2$ in the RWG obtained with θ = 3.00° (off-resonance).

and it reveals that the transmittance minimum (GMR) appears at λ = 950 nm for θ = 0°. When the incident angle increases, the GMR mode splits into two separate branches; one branch blue-shifts with the incident angle and the other red-shifts. The latter one can be used for resonant excitation of the sample, which takes place at λ = 976 nm and θ = 2.75°. Figure 4b shows the measured and calculated transmission spectra of the sample obtained at θ = 2.75°, and it is evident that both spectra yield the same GMR wavelengths. To investigate how the UCL signal is affected by resonant excitation, we measured UCL spectra of the sample obtained with resonant and nonresonant excitation conditions. In this investigation, a continuous wave (CW) collimated laser beam (beam diameter = 1.8 mm) at 976 nm with a power of 600 mW was employed to excite the RWG area of the sample at θ = 2.75° (on-resonance), θ = 3.00° (off-resonance), and non-RWG (nongrating) area of the sample. The UCL emission at detection angle ϕ = 15° was collected and delivered to a grating spectrometer for analysis. Figure 4c shows the results of the UCL measurement and it is clear that the UCL emission obtained with θ = 2.75° is much stronger than those of obtained with θ = 3.00° and non-RWG area. The inset in Figure 4c shows optical images of the UCL emission at RWG area of the sample taken at on-resonance and off-resonance excitation conditions, where the circled region in each image is the lateral range of the RWG structure. It is surprising that the UCL emission has such a dramatic difference when the excitation angle is slightly tuned 0.25° away from the resonant excitation angle. This phenomenon can be explained by comparing the excitation electric field intensity distributions in these two cases. As the sample is excited under resonance condition (θ = 2.75°), a strong electric field is built atop of the TiO_2 surface (see Figure 1b) where UCNPs are deposited, and thus it produces very strong UCL emission. However, when the excitation angle is slightly increased to 3.00°, the electric field atop of the TiO_2 surface is dramatically decreased (see Figure 4d), which results in a relatively low intensity of UCL output.

In order to further evaluate the influence of the structure parameters of the RWG on the UCL, we measured the UCL spectra of three samples under their excitation resonance conditions. First, we compared the UCL emission intensities of UCNPs deposited atop of the SU-8 and low-n RWGs (see Figure 5). The SU-8 RWG has the same structure parameters

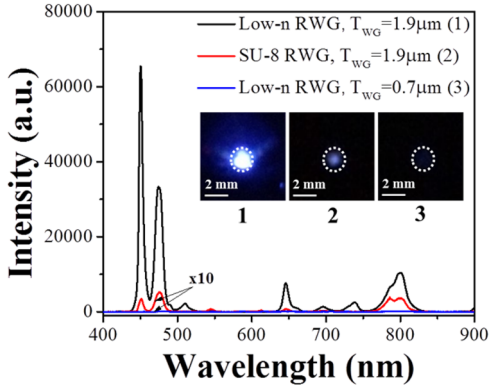

Figure 5. UCL spectra of the UCNPs deposited atop of RWGs under resonant excitation low-n RWG with two different thicknesses (T_{WG} = 1.9 and 0.7 μm) and SU-8 RWG with T_{WG} = 1.9 μm. Insets show optical images of the UCL emission of the samples taken under resonant excitation condition.

as those of the aforementioned low-n RWG, except the low-n mesoporous silica layer of the low-n RWG was replaced by the SU-8 layer. Figure 5 clearly displays the UCL intensity of UCNPs atop of the low-n RWG is much stronger that of UCNPs on the surface of the SU-8 RWG. The emission peak intensity at 450 nm of the former is about 190× higher than that of the latter. This result confirms that the low-n RWG can produce stronger local electric field on its top surface, which agrees with the simulation result shown in Figure 1. Furthermore, we compared UCL intensities of UCNPs atop of the low-n RWG with two different thicknesses of the low-n mesoporous silica layer (T_{WG} = 0.7 and 1.9 μm) under resonant excitation condition. As shown in Figure 5, the UCL emission obtained from the low-n RWG with T_{WG} = 1.9 μm is much stronger than that obtained with T_{WG} = 0.7 μm. It implies that the low-n RWG with T_{WG} = 1.9 μm indeed can yield stronger local electric filed atop of its surface, same as the simulation prediction displayed in Figure 2a.

The UCL emission intensity can be further enhanced by the extraction resonance effect,[23] through tuning the detection angle (ϕ) to have GMR wavelength overlap with the UCL emission wavelength. To observe the phenomenon, the UCL emission spectra of UCNPs deposited atop of the low-n RWG were measured by varying the detection angle from 13° to 73° while the incident angle of the excitation laser beam was fixed at

DOI: 10.1021/acsphotonics.8b00494
ACS Photonics 2018, 5, 3263−3271

θ = 2.75° (resonant excitation angle). Figure S2a shows the UCL intensities of three emission peaks (450, 480, 645 nm) versus the detection angle. As displayed, UCL intensities of these three peaks are enhanced 2−4× at particular detection angle ϕ, where ϕ = 30° and 26° for 645 nm emission, ϕ = 59°, 49°, and 40° for 480 nm emission, and ϕ = 52° and 32° for 450 nm emission. By examining the angle-resolved transmission spectra shown in Figure S2b−d, a GMR mode, which has the same resonance wavelength as the UCL emission, can be found at each of the aforementioned ϕ angles.

We studied the excitation intensity dependence of the UCL emission intensities of the UCNPs deposited low-n RWG sample. Figure S3c displays the logarithmic plot of the UCL emission intensities versus the excitation intensity in the range of 1−6 W/cm^2 obtained under excitation resonance condition, and under simultaneous excitation and extraction resonance, respectively. As revealed in Figure S3a, the UCL emission intensity of each peak is proportional to the nth power of the excitation intensity, where n are 3.55, 2.41, and 2.44 for the emission peaks at 450, 480, and 645 nm, respectively. Similarly, the corresponding power exponents n are 3.35, 2.22, and 2.15 for the case of simultaneous excitation and extraction resonance (see Figure S3b). These n values suggest that the $^1D_2$ state and the $^1G_4$ state of Tm^{3+} ions are populated via four-photon and three-photon processes, respectively, agreeing with previously findings.[23,32−34] For comparison, the result obtained from the non-RWG sample with excitation intensity in the range of 18−220 W/cm^2 is shown in Figure S3c. Since the UCL signal generated from the non-RWG sample with a collimated excitation beam is too weak to detect, a convex lens with focus length of 20 cm was used to focus the excitation laser beam into a spot of 0.3 mm diameter on the non-RWG sample to increase the excitation intensity. The corresponding n values, obtained from Figure S3c, are 2.69, 1.97, and 1.71. These values are smaller than those obtained from the cases of excitation resonance and simultaneous excitation and extraction resonance, which is consistent with our previous results.[23] The reduction of n values has been reported for the case of high excitation intensity.[35,36] However, this is not the reason for the non-RWG sample to have smaller n values. Although exposure of excitation intensity to the RWG sample was lower than that of exposed to the non-RWG sample, after considering the electric field intensity enhancement atop of the RWG under resonant excitation as shown in Figures 1b and 2, the excitation intensities experienced by both samples were actually close. According to the simple models presented (refs 35 and 36), the power exponent depends on the relative magnitude of the excitation rate of Tm^{3+} ions and the rates at which the excited Tm^{3+} ions decay. For a given excitation intensity, excited Tm^{3+} ions with higher decay rate yield larger power exponent and vice versa. Figure S3d shows the decay of the UCL emission, produced from the $^1D_2$ state at 450 nm, obtained from the non-RWG area and the RWG area under excitation resonance and simultaneous excitation and extraction resonance. As depicted, the lifetime of the RWG sample is shorter (163 and 143 μs) than that of the non-RWG sample (210 μs). In other words, the decay rate of the $^1D_2$ state of Tm^{3+} ions is higher for the RWG sample compared to the non-RWG sample, which thus yields larger n values for the RWG sample.

To determine the UCL enhancement factors produced from the low-n RWG sample, we have to choose a proper excitation intensity that can generate detectable UCL signal from both RWG and non-RWG samples. However, the lowest excitation intensity to generate detectable UCL signal from the non-RWG sample is about 18 W/cm^2, which is still higher than the highest excitation intensity (about 6 W/cm^2) that we can obtain for the collimated NIR laser used to pump the RWG sample. Thus, we extrapolated the UCL intensities of the non-RWG sample to the excitation intensity of 6 W/cm^2 proceed from the power exponents obtained at higher excitation intensity (see Figure S3c). The UCL intensities obtained at 6 W/cm^2 (marked by vertical dot lines in Figure S3a−c) were chosen to determine the UCL enhancement factors, defined as the ratio of UCL intensity generated from the RWG sample to that of the non-RWG sample. Table 1 summaries the UCL enhancement factors of the low-n RWG at three main emission wavelengths. For the case of excitation resonance, the enhancement factors for emission wavelengths (λ_e) at 450, 480, and 645 nm are 8.4 × 10^4, 1.2 × 10^4, and 6.4 × 10^3, respectively. For the case of simultaneous excitation and extraction resonance, they are 21.4 × 10^4, 2.9 × 10^4, and 2.8 × 10^4, respectively. The UCL enhancement factors obtained in this work are about 2−3 orders of magnitude higher than those obtained by other methods, for example, material improvements,[11−15] photonic crystal effect,[16,17] and plasmonic effect.[18−22] The strong UCL emission obtained in this work is attributed to the build-up of strong local field atop of the low-n RWG under excitation resonance, which effectively increases NIR absorption of UCNPs. In addition, large power exponent dependence between excitation intensity and UCL emission intensity, associated with four-photon or three-photon absorption transition experienced by Tm^{3+} ions and low-n RWG, is another factor that gives rise to highly efficient UCL emission.

Table 1. Summary of Enhancement Factors of Three Emission Wavelengths (λ_e) at 450, 480, and 645 nm of the UCNPs Deposited Atop of the Low-n RWG under Excitation Resonance and Simultaneous Excitation and Extraction Resonance

	enhancement factor		
λ_e (nm)	450	480	645
excitation resonance	8.4 × 10^4	1.2 × 10^3	6.4 × 10^3
excitation and extraction resonance	21.4 × 10^4	2.9 × 10^4	2.8 × 10^4

To evaluate the feasibility of using low-n RWG in UCL biosensing and bioimaging applications, UCNPs-SA were used as bioprobes to detect biotin molecules on the low-n RWG. Specifically, biotin moieties were conjugated onto the TiO_2 surface of the low-n RWG via a chemical modification process with (3-aminopropyl)triethoxysilane (APTES). Then, the biotinalyted low-n RWG was incubated with UCNPs-SA for the next step of UCL emission measurement (see Figure 6a). To confirm streptavidin molecules were successfully conjugated to UCNPs, the Fourier-transform infrared spectroscopy (FTIR) spectra and zeta potentials of poly(acrylic acid) (PAA)-functionalized $NaYF_4$:Yb^{3+},Tm^{3+} nanoparticles (UCNPs-PAA) and UCNPs-SA were compared. Figure S4a shows the FTIR spectra of UCNPs-PAA (curve a) and UCNPs-SA (curve b). The strong peak at 1639 cm^{-1} in both curves corresponds to the COO-symmetrical stretching vibration.[37] Figure S4b shows the difference between curves a and b, which clearly illustrates the peaks associated with the amide bands II (1546 cm^{-1}) and I (1697 cm^{-1}) of streptavidin.[38] It proves that streptavidin molecules were successfully conjugated onto the

DOI: 10.1021/acsphotonics.8b00494
ACS Photonics 2018, 5, 3263−3271

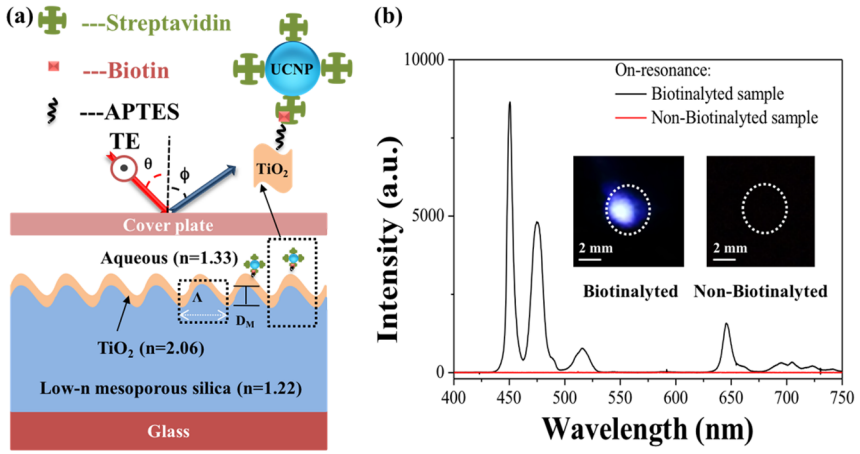

Figure 6. (a) Schematic of the low-n RWG sample. Its top surface was first deposited with UCNPs by streptavidin−biotin interaction method, then covered with aqueous solution. θ and ϕ are the excitation beam incident angle and the UCL detection angle relative to the surface normal direction, respectively. (b) UCL emission spectra of the UCNPs-SA after drop-casting atop of the biotinylated and nonbiotinylated low-n RWGs obtained at on-resonance condition (θ = 1.5°).

surface of the UCNPs. Figure S4c shows the zeta potentials of UCNPs-PAA and UCNPs-SA. It clearly displays a change of zeta potentials of these two samples (ζ = −35.7 to −14.3 mV), which further confirms the formation of streptavidin-functionalized UCNPs. To verify the success of conjugation of biotin moieties onto TiO_2 surface, we measured the FTIR spectra of TiO_2 samples before and after the conjugation of biotin moieties (see Figure S4d). It clearly displays the change of IR absorption before and after the surface modification. For the untreated TiO_2, we did not find any IR absorption band related to functional groups of biotin. After the surface treatment, the peaks at 1648 and 1460 cm^{-1}, associated with the $-NH_2$ and −CH stretching vibrations, respectively, were found. In addition, the peaks corresponding to the amide I and amide II were observed.[39] These results suggest that the biotin moieties were successfully attached onto the surface of TiO_2 surface.

Figure 6b shows the UCL spectra of UCNPs-SA after drop-casting atop of the biotinylated and nonbiotinylated low-n RWGs obtained under excitation resonance condition. Obviously, the UCL emission generated from the biotinylated low-n RWG is much stronger than that generated from the nonbiotinylated low-n RWG. Since the local field enhancement factors produced atop of the TiO_2 surface of both samples are quite similar, the UCL emission strength difference between these two samples should be resulted from the difference of the number of UCNPs-SA attached to the TiO_2 surface of both samples. It indicates that higher number of UCNPs-SA are immobilized on the top surface of the biotinylated low-n RWG thanks to the specific bonding between biotin and streptavidin. In contrast, no or very low number of UCNPs-SA are attached atop of the nonbiotinylated low-n RWG because of the lack of biotin and streptavidin interaction. The strong UCL emission result also implies that biotin can be effectively detected through the use of low-n RWG and UCNPs-SA and it confirms that the low-n RWG has high potential for UCL biosensing and bioimaging applications.

CONCLUSIONS

In this work, we demonstrate higher than 10^4-fold enhancement of UCL of Tm^{3+}-doped UCNPs in aqueous solution by utilizing a low-n RWG. Through RCWA simulation, the structure parameters of the low-n RWG are tuned to yield strong local electric field atop of the low-n RWG, where UCNPs are deposited. When the excitation light at 976 nm overlaps with the GMR, the largest enhancement factor (about 10^4 times) of UCL emission of Tm^{3+}-doped UCNPs on the low-n RWG substrate is obtained, which is due to the resonant excitation effect. Furthermore, the extraction of the UCL emissions is improved 2−4 fold on the basis of overlapping the emission wavelengths with their associated GMR wavelengths. We emphasize that using low-n RWG is prerequisite for enhancing UCL emission of UCNPs in aqueous environment, thus being feasible for many applications in biomedicine. Our strategy exploits the advantage of using low-n RWG in versatile biosensing and bioimaging applications. For example, we employ the streptavidin-linked UCNPs as UCL bioprobes for facile detection of biotin molecules atop of the low-n RWG. We believe that our results can open up effective avenue to enhance UCL efficiency of UCNPs in aqueous solution and is therefore advantageous for board range of applications based on their extraordinary enhanced UCL emission.

MATERIALS AND METHODS

Chemicals. Yttrium(III) chloride (YCl_3, anhydrous powder, 99.99%), ytterbium(III) chloride ($YbCl_3$, anhydrous powder, 99.9%), thulium(III) chloride ($TmCl_3$, anhydrous powder, 99.9%), and ammonium fluoride (NH_4F, anhydrous 99,99%) were purchased from Sigma-Aldrich and stored in a drybox. Sodium oleate (97%) was purchased from TCI America. Oleic acid (OA, technical grade, 90%), 1-octadecene (ODE, technical grade, 90%), tetraethyl orthosilicate (TEOS, 98%), (3-aminopropyl) triethoxysilane (APTES, 98%), *N*-(3-dimethylaminopropyl)-*N*-ethylcarbodiimide hydrochloride (EDC), *N*-hydroxysuccinimide (NHS, ≥97%), poly(acrylic acid) (PAA, $M_w \approx$ 1800), and biotin (≥99%) were purchased from Sigma-Aldrich. Streptavidin protein was purchased from Rockland Immunochemicals Inc. and stored at −20 °C.

Synthesis of $NaYF_4$:Yb^{3+},Tm^{3+} UCNPs. Monodispersed $NaYF_4$:Yb^{3+},Tm^{3+} UCNPs were synthesized through a thermal decomposition process with a slight modification.[40] A typical procedure is as follows: a mixture of 0.78 mmol of YCl_3, 0.2 mmol of $YbCl_3$, 0.02 mmol of $TmCl_3$, 6 mL of OA, and 15 mL of ODE were added into a 100 mL circle bottom flask. The

DOI: 10.1021/acsphotonics.8b00494
ACS Photonics 2018, 5, 3263−3271

resulting mixture was heated to 160 °C with vigorous magnetic stirring until the solution was clear under a nitrogen flow, and then placed under vacuum and heated to 110 °C for 1 h. After the solution was cooled down to the room temperature, 0.76 g sodium oleate was added and 10 mL of methanol solution containing NH_4F (0.148 g) was slowly added dropwise into the flask and stirred for 30 min. After that, the solution was slowly heated to 110 °C for 10 min to remove methanol, and then placed under vacuum and heated to 110 °C for 1 h. Under a nitrogen atmosphere, the solution was heated to 300 °C and maintained for 45 min and then cooled rapidly by a strong stream of nitrogen gas to the outside of the flask following exclusion from the heating mantle. Finally, UCNPs capped with oleic acid from the solution were centrifuged at 6000 rpm for 10 min to precipitate the nanoparticles completely. This washing procedure was repeated two more times to ensure washing of the reaction surfactants as well as any previously created NaF impurities.

Preparation of Hydrophilic $NaYF_4$:Yb^{3+},Tm^{3+} Nanoparticles. The PAA-functionalized $NaYF_4$:Yb^{3+},Tm^{3+} nanoparticles were prepared by using a modified ligand exchange strategy.[18] The procedure is as follows: the mixture containing 1 mL of PAA solution in ethanol (~1 wt %) and 0.5 mL of UCNPs dispersed in chloroform (~1 wt %) was stirred for 12 h. The nanoparticles were then isolated via centrifugation at 7000 rpm for 30 min. After being further purified at least three times with absolute ethanol/deionized water (1:1 v/v), the particles could be redispersed readily in water to form a transparent colloidal solution without any obvious precipitation for more than two months.

Preparation of Streptavidin-Functionalized UCNPs. Streptavidin-functionalized $NaYF_4$:Yb^{3+},Tm^{3+} UCNPs were prepared via the following protocol: 5 mg of UCNPs-PAA were suspended in 1 mL of 2-(N-morpholino) ethanesulfonic acid (MES) buffer (pH = 5.5) containing EDC (1 mg/mL) and NHS (0.5 mg/mL) and soaked at room temperature for 2 h to activate the carboxylic acid groups. After centrifugation and being washed with phosphate-buffered saline (PBS) buffer (pH = 7.4), the precipitate was added to 1 mL of PBS buffer containing 300 μL of streptavidin solution (concentration: 5×10^{-8} g/mL). The linkage reaction was allowed to proceed at room temperature for 5 h. The UCNPs-SA were then isolated via centrifugation at 14000 rpm for 30 min and then dispersed in 1 mL of PBS buffer and kept at 4 °C for further applications.

Fabrication of UCNPs Deposited Low-n RWG Structure. The low-n RWG structure was fabricated using a combination of interference lithography, molding, and imprint processes. Typically, a one-dimensional SU-8 photoresist grating was first fabricated on top of a glass substrate by a two-beam interference technique.[41] Then, we replicated the SU-8 grating mold by casting polydimethylsiloxane (PDMS) precursor liquid containing prepolymer (part A) and curing agent (part B) with a mix mass ratio of 10:1. The PDMS precursor liquid was poured onto the top of the SU-8 master mold placed into a glass Petri-dish and then held at 50 °C for 12 h. The PDMS flexible mold was then used to imprint the grating structure onto a low-n mesoporous silica thin film.

Low-n mesoporous silica thin films were prepared by using block copolymers poly(ethylene oxide-*b*-3-caprolactone) (PEO-*b*-PCL) and poly(ethylene oxide-*b*-propylene oxide-*b*-ethylene oxide) (F127) as cotemplates, TEOS as the silica precursor, hydrochloric acid (HCl) as catalysis, and tetrahydrofuran (THF) as solvent.[42] The following parameters were used for a typical fabrication procedure: TEOS (0.6 g) and 0.1 M HCl (2 g) were added to a THF solution (5 g) containing diblock copolymer PEO-*b*-PCL (0.14 g) and the triblock copolymer F127 (0.18 g). Next, the reaction solution was magnetically stirred for 30 min and kept at a room temperature. The resulting homogeneous solution was spin-coated (1500 rpm, 80 s) onto a glass substrate. A two-step baking, first in air at 50 °C for 2 min, then followed by 200 °C for 10 min, was applied to form a mesoporous silica thin film. In the case of thick films, multiple coatings were processed for eight times to obtain the desired thickness (about 2 μm). Then, the PDMS flexible mold was employed to imprint a grating structure atop of the low-n mesoporous silica thin film by nanoimprint technique. The RWG structure was obtained by subsequent deposition of a high refractive index TiO_2 thin film on the imprinted area by the electron-beam deposition technique. Finally, the pure $NaYF_4$:Yb^{3+},Tm^{3+} UCNPs were deposited onto the top surface (TiO_2 layer) of the RWG structure by dip-coating method and then baking at 80 °C for 1 h on a hot plate. The experimental process for the multilayer low-n mesoporous silica thin film and low-n RWG using imprinting method can be seen in Figure S5.

Preparation of Biotinalyted Low-n RWG Structure. First, the untreated TiO_2 surface of the low-n RWG was exposed to oxygen plasma treatment to create the hydrophilic surface in the form of Ti−OH through oxidation of TiO_2 by O_2 plasma and dissociative adsorption of water molecules in the atmosphere.[43,44] The hydroxylated TiO_2 surface was functionalized by immersing in a mixture of APTES and anhydrous ethanol (volume ratio = 3:1000) for 16 h to generate an amino group on the TiO_2 layer.[43] Subsequently, the amino-silanized surface was biotinylated by reacting with biotin through EDC/NHS chemistry (1 mL of 1 mg/mL biotin) for 2 h at 4 °C. The unreacted EDC and NHS were then rinsed out with ethanolamine/deionized water solvent mixture. Finally, the resulting samples were then redispersed into PBS buffer and stored at 4 °C for further use.

Detection of Biotin. Both the biotinylated and non-biotinylated low-n RWG samples were incubated with 400 μL of 5 mg/mL of UCNPs-SA in PBS buffer for 50 min (note that longer incubation time did not result in more adsorption of UCNPs-SA on substrate) at room temperature. The UCNPs-SA were conjugated to the biotinylated TiO_2 surface through the specific biotin−streptavidin interaction. Then, the samples were placed in a Petri-dish filled with deionized water and rinsed with a vortex stirrer at a speed of 800 rpm for 15 min to remove the unbound particles. After the samples were encapsulated with the cover plate, UCL spectra were measured and analyzed.

UCL and Lifetime Measurement. The excitation source for UCL and lifetime measurements was a NIR CW diode laser at 976 nm (Thorlab BL976-PAG900) with a spectral bandwidth of <1 nm. The output beam was collimated by using a fiber collimator (F220APC-980) with a beam diameter of 1.8 mm. To adjust the excitation power down to the required level, the laser beam was passed through a variable attenuator composed of the combination of a half-wave plate and a polarizer. UCL spectra were detected by a grating spectrometer (Andor Shamrock SR-500i) adopted with a fiber coupler. Before the UCL signal was sent through the fiber coupler, an IR filter was used to block the excitation laser light. For the lifetime measurement, a mechanical chopper was employed to turn on and off the excitation laser light, and the UCL signal

DOI: 10.1021/acsphotonics.8b00494
ACS Photonics 2018, 5, 3263−3271

was collected and directed to a photomultiplier tube (PMT) with a pair of lenses. To ensure only desired UCL single was detected, a suitable interference filter at a specific wavelength was placed in front of the PMT to block excitation laser light and undesired UCL emission.

Simulation. Rigorous coupled-wave analysis[45,46] was used to calculate transmission spectra and electric-field intensity distributions in the low-n RWG and SU-8 RWG. In our calculation, the unit cell used for simulations was defined as one period of the device (as illustrated in dashed rectangle in Figure 3a). The incident light was set to be transverse electric polarization and the harmonics were retained at 25 in both the x and z directions.

Characterization. The crystalline phase of UCNPs was measured with a Bruker APEX diffractometer (λ = 1.5406 Å). Morphology of nanoparticles were characterized with TEM (JEOL-JEM 2010) and high resolution TEM (HR-TEM, JEOL, JEM-2100). Meanwhile, the FTIR spectra of as-prepared samples, which were dispersed in KBr pellets, were measured with a Varian FTIR-640 spectrometer equipped with a liquid nitrogen-cooled mercury−cadmium-telluride (MCT) detector. The thickness of the low-n mesoporous silica film was determined with the α step (Bruker Dimension Icon). The modulation depth and grating period were measured with the atomic force microscopy (AFM Park Systems XE-70). The transmission spectra of the low-n RWG, whose top surface was deposited with UCNPs and covered with aqueous solution, were measured with the grating spectrometer (Andor Shamrock SR-500i).

■ ASSOCIATED CONTENT

Supporting Information

The Supporting Information is available free of charge on the ACS Publications website at DOI: 10.1021/acsphotonics.8b00494.

The fabrication scheme of the low-n RWG and physical properties of $NaYF_4$:Yb^{3+},Tm^{3+} UCNPs (TEM image, XRD pattern, and UCL spectra), extraction resonance and excitation intensity dependences of the UCNPs deposited low-n RWG (PDF).

■ AUTHOR INFORMATION

Corresponding Author

*E-mail: phycch@ccu.edu.tw.

ORCID

Shiao-Wei Kuo: 0000-0002-4306-7171

Lai-Kwan Chau: 0000-0002-1659-6465

Chia-Chen Hsu: 0000-0002-3014-8829

Author Contributions

C.C.H. planned the project and supervised the overall project. D.T.V. performed the simulation, performed all the experiments, and the synthesis of the UCNPs. H.W.C. and R.N. fabricated and modified surface of the low-n RWG. Q.M.L. and C.C.T. instructed the synthesis of UCNPs. S.W.K. instructed the fabrication of low-n thin film. L.K.C. contributed to the idea of the surface modification of low-n RWG. H.C.K. instructed to perform the simulation and the coating of TiO_2 thin film. The manuscript was written through contributions of all authors.

Notes

The authors declare no competing financial interest.

■ ACKNOWLEDGMENTS

The authors gratefully acknowledge financial support from the Ministry of Science and Technology, Taiwan, under Grant Nos. MOST 107-2923-M-194-001-MY3 and MOST 104-2112-M-194-002-MY3.

■ REFERENCES

(1) Wang, F.; Liu, X. Recent advances in the chemistry of lanthanide-doped upconversion nanocrystals. *Chem. Soc. Rev.* **2009**, *38*, 976−989.

(2) Haase, M.; Schafer, H. Upconverting Nanoparticles. *Angew. Chem., Int. Ed.* **2011**, *50*, 5808−5829.

(3) Chen, C.; Li, C.; Shi, Z. Current Advances in Lanthanide-Doped Upconversion Nanostructures for Detection and Bioapplication. *Adv. Sci.* **2016**, *3*, 1600029.

(4) Lim, S. F.; Riehn, R.; Ryu, W. S.; Khanarian, N.; Tung, C. K.; Tank, D.; Austin, R. H. In Vivo and Scanning Electron Microscopy Imaging of Upconverting Nanophosphors in Caenorhabditis elegans. *Nano Lett.* **2006**, *6*, 169−174.

(5) Wang, F.; Banerjee, D.; Liu, Y.; Chen, X.; Liu, X. Upconversion nanoparticles in biological labeling, imaging, and therapy. *Analyst* **2010**, *135*, 1839−1854.

(6) Xu, S.; Xu, S.; Zhu, Y.; Xu, W.; Zhou, P.; Zhou, C.; Dong, B.; Song, H. A novel upconversion, fluorescence resonance energy transfer biosensor (FRET) for sensitive detection of lead ions in human serum. *Nanoscale* **2014**, *6*, 12573−12579.

(7) Heer, S.; Kompe, K.; Gudel, H. U.; Haase, M. Higly Efficient Multicolor Upconversion Emission in Transparent Colloids of Lanthanide-Doped $NaYF_4$ Nanocrystals. *Adv. Mater.* **2004**, *16*, 2102−2105.

(8) Wang, F.; Liu, X. Upconversion Multicolor Fine-Tuning: Visible to Near-Infrared Emission from Lanthanide-Doped $NaYF_4$ Nanoparticles. *J. Am. Chem. Soc.* **2008**, *130*, 5642−5643.

(9) Ye, X.; Collins, J. E.; Kang, Y.; Chen, J.; Chen, D. T. N.; Yodh, A. G.; Murray, C. B. Morphologically controlled synthesis of colloidal upconversion nanophosphors and their shape-directed self-assembly. *Proc. Natl. Acad. Sci. U. S. A.* **2010**, *107*, 22430−22435.

(10) Boyer, J. C.; van Veggel, F. C. Absolute quantum yield measurements of colloidal $NaYF_4$:Er^{3+},Yb^{3+} upconverting nanoparticles. *Nanoscale* **2010**, *2*, 1417−1419.

(11) Zhao, J.; Jin, D.; Schartner, E. P.; Lu, Y.; Liu, Y.; Zvyagin, A. V.; Zhang, L.; Dawes, J. M.; Xi, P.; Piper, J. A.; Goldys, E. M.; Monro, T. M. Single-nanocrystal sensitivity achieved by enhanced upconversion luminescence. *Nat. Nanotechnol.* **2013**, *8*, 729−734.

(12) Wisser, M. D.; Fischer, S.; Maurer, P. C.; Bronstein, N. D.; Chu, S.; Alivisatos, A. P.; Salleo, A.; Dionne, J. A. Enhancing Quantum Yield via Local Symmetry Distortion in Lanthanide-Based Upconverting Nanoparticles. *ACS Photonics* **2016**, *3*, 1523−1530.

(13) Han, S.; Deng, R.; Xie, X.; Liu, X. Enhancing Luminescence in Lanthanide-Doped Upconversion Nanoparticles. *Angew. Chem., Int. Ed.* **2014**, *53*, 11702−11715.

(14) Zhou, B.; Tao, L.; Tsang, Y. H.; Jin, W. Core−shell nanoarchitecture: a strategy to significantly enhance white-light upconversion of lanthanide-doped nanoparticles. *J. Mater. Chem. C* **2013**, *1*, 4313−4318.

(15) Chen, G.; Ågren, H.; Ohulchanskyy, T. Y.; Prasad, P. N. Light upconverting core−shell nanostructures: nanophotonic control for emerging applications. *Chem. Soc. Rev.* **2015**, *44*, 1680−1713.

(16) Yin, Z.; Zhu, Y.; Xu, W.; Wang, J.; Xu, S.; Dong, B.; Xu, L.; Zhang, S.; Song, H. Remarkable enhancement of upconversion fluorescence and confocal imaging of PMMA Opal/$NaYF_4$:Yb^{3+},Tm^{3+}/Er^{3+} nanocrystals. *Chem. Commun.* **2013**, *49*, 3781−3783.

(17) Liao, J.; Yang, Z.; Lai, S.; Shao, B.; Li, J.; Qiu, J.; Song, Z.; Yang, Y. Upconversion Emission Enhancement of $NaYF_4$:Yb,Er Nanoparticles by Coupling Silver Nanoparticle Plasmons and Photonic Crystal Effects. *J. Phys. Chem. C* **2014**, *118*, 17992−17999.

(18) Kannan, P.; Rahim, F. A.; Teng, X.; Chen, R.; Sun, H.; Huang, L.; Kim, D. H. Enhanced emission of $NaYF_4$:Yb,Er/Tm nanoparticles

DOI: 10.1021/acsphotonics.8b00494
ACS Photonics 2018, 5, 3263−3271

by selective growth of Au and Ag nanoshells. *RSC Adv.* **2013**, *3*, 7718−7721.
(19) He, J.; Zheng, W.; Ligmajer, F.; Chan, C. F.; Bao, Z.; Wong, K. L.; Chen, X.; Hao, J.; Dai, J.; Yu, S. F.; Lei, D. Y. Plasmonic enhancement and polarization dependence of nonlinear upconversion emissions from single gold nanorod@SiO_2@CaF_2:Yb^{3+},Er^{3+} hybrid core−shell−satellite nanostructures. *Light: Sci. Appl.* **2016**, *6*, 16217.
(20) Xu, W.; Min, X.; Chen, X.; Zhu, Y.; Zhou, P.; Cui, S.; Xu, S.; Tao, L.; Song, H. Ag-SiO_2-Er_2O_3. Nanocomposites: Highly Effective Upconversion Luminescence at High Power Excitation and High Temperature. *Sci. Rep.* **2015**, *4*, 5087.
(21) Schietinger, S.; Aichele, T.; Wang, H. Q.; Nann, T.; Benson, O. Plasmon-Enhanced Upconversion in Single $NaYF_4$:Yb^{3+}/Er^{3+} Co-doped Nanocrystals. *Nano Lett.* **2010**, *10*, 134−138.
(22) Zhang, W.; Ding, F.; Chou, S. Y. Large Enhancement of Upconversion Luminescence of $NaYF_4$:Yb^{3+}/Er^{3+} Nanocrystal by 3D Plasmonic NanoAntennas. *Adv. Mater.* **2012**, *24*, 236−241.
(23) Lin, J. H.; Liou, H. Y.; Wang, C. D.; Tseng, C. Y.; Lee, C. T.; Ting, C. C.; Kan, H. C.; Hsu, C. C. Giant Enhancement of Upconversion Fluorescence of $NaYF_4$:Yb^{3+},Tm^{3+} Nanocrystals with Resonant Waveguide Grating Substrate. *ACS Photonics* **2015**, *2*, 530−536.
(24) Hasnain, C. J. C.; Yang, W. High-contrast gratings for integrated optoelectronics. *Adv. Opt. Photonics* **2012**, *4*, 379−440.
(25) Collin, S. Nanostructure arrays in free-space: optical properties and applications. *Rep. Prog. Phys.* **2014**, *77*, 126402.
(26) Ganesh, N.; Zhang, W.; Mathias, P. C.; Chow, E.; Soares, J. A. N. T.; Malyarchuk, V.; Smith, A. D.; Cunningham, B. T. Enhanced fluorescence emission from quantum dots on a photonic crystal surface. *Nat. Nanotechnol.* **2007**, *2*, 515−520.
(27) Lin, J. H.; Tseng, C. Y.; Lee, C. T.; Kan, H. C.; Hsu, C. C. Guided-mode resonance enhanced excitation and extraction of two-photon photoluminescence in a resonant waveguide grating. *Opt. Express* **2013**, *21*, 24318−24325.
(28) Lin, J. H.; Tseng, C. Y.; Lee, C. T.; Young, J. F.; Kan, H. C.; Hsu, C. C. Strong guided mode resonant local field enhanced visible harmonic generation in an azopolymer resonant waveguide grating. *Opt. Express* **2014**, *22*, 2790−2797.
(29) Horvath, R.; Pedersen, H. C. Demonstration of reverse symmetry waveguide sensing in aqueous solutions. *Appl. Phys. Lett.* **2002**, *81*, 2166−2168.
(30) Horvath, R.; Lindvold, L. R.; Larsen, N. B. Reverse-symmetry waveguides: theory and fabrication. *Appl. Phys. B: Lasers Opt.* **2002**, *74*, 383−393.
(31) Block, I. D.; Chan, L. L.; Cunningham, B. T. Photonic crystal optical biosensor incorporating structured low-index porous dielectric. *Sens. Actuators, B* **2006**, *120*, 187−193.
(32) Wei, Y.; Lu, F.; Zhang, X.; Chen, D. Synthesis and characterization of efficient near-infrared upconversion Yb and Tm codoped $NaYF_4$ nanocrystal reporter. *J. Alloys Compd.* **2007**, *427*, 333−340.
(33) Wang, G.; Qin, W.; Wang, L.; Wei, G.; Zhu, P.; Kim, R. Intense ultraviolet upconversion luminescence from hexagonal $NaYF_4$:Yb^{3+}/Tm^{3+} microcrystals. *Opt. Express* **2008**, *16*, 11907−11914.
(34) Qiu, H.; Yang, C.; Shao, W.; Damasco, J.; Wang, X.; Ågren, H.; Prasad, P. N.; Chen, G. Enhanced upconversion luminescence in Yb^{3+}/Tm^{3+}-codoped fluoride active core/active shell/inert shell nanoparticles through directed energy migration. *Nanomaterials* **2014**, *4*, 55−68.
(35) Pollnau, M.; Gamelin, D. R.; Lüthi, S. R.; Güdel, H. U.; Hehlen, M. P. Power dependence of upconversion luminescence in lanthanide and transition-metal-ion systems. *Phys. Rev. B: Condens. Matter Mater. Phys.* **2000**, *61*, 3337−3346.
(36) Suyver, J. F.; Aebischer, A.; García-Revilla, S.; Gerner, P.; Güdel, H. U. Anomalous power dependence of sensitized upconversion luminescence. *Phys. Rev. B: Condens. Matter Mater. Phys.* **2005**, *71*, 125123.
(37) Xia, A.; Deng, Y.; Shi, H.; Hu, J.; Zhang, J.; Wu, S.; Chen, Q.; Huang, X.; Shen, J. Polypeptide-Functionalized $NaYF_4$:Yb^{3+},Er^{3+} Nanoparticles: Red Emission Biomarkers for High Quality Bioimaging Using a 915 nm Laser. *ACS Appl. Mater. Interfaces* **2014**, *6*, 18329−18336.
(38) Dong, H.; Yan, F.; Ji, H.; Wong, D. K. Y.; Ju, H. Quantum-Dot-Functionalized Poly(styrene-co-acrylic acid) Microbeads: Step-Wise Self-Assembly, Characterization, and Applications for Sub-femtomolar Electrochemical Detection of DNA Hybridization. *Adv. Funct. Mater.* **2010**, *20*, 1173−1179.
(39) Ye, L.; Pelton, R.; Brook, M. A. Biotinylation of TiO_2 Nanoparticles and Their Conjugation with Streptavidin. *Langmuir* **2007**, *23*, 5630−5637.
(40) Li, Z.; Zhang, Y.; Jiang, S. Multicolor Core/Shell-Structured Upconversion Fluorescent Nanoparticles. *Adv. Mater.* **2008**, *20*, 4765−4769.
(41) Lai, N. D.; Liang, W. P.; Lin, J. H.; Hsu, C. C.; Lin, C. H. Fabrication of two- and three-dimensional periodic structures by multi-exposure of two-beam interference technique. *Opt. Express* **2005**, *13*, 9605−9611.
(42) Liu, C. C.; Li, J. G.; Kuo, S. W. Co-template method provides hierarchical mesoporous silicas with exceptionally ultra-low refractive indices. *RSC Adv.* **2014**, *4*, 20262−20272.
(43) Kim, W. J.; Kim, S.; Lee, B. S.; Kim, A.; Ah, C. S.; Huh, C.; Sung, G. Y.; Yun, W. S. Enhanced Protein Immobilization Efficiency on a TiO_2 Surface Modified with a Hydroxyl Functional Group. *Langmuir* **2009**, *25*, 11692−11697.
(44) Wang, D.; Chen, A.; Jang, S. H.; Yip, H. L.; Jen, A. K. Y. Sensitivity of titania(B) nanowires to nitroaromatic and nitroamino explosives at room temperature via surface hydroxyl groups. *J. Mater. Chem.* **2011**, *21*, 7269−7273.
(45) Moharam, M. G.; Gaylord, T. K. Rigorous coupled-wave analysis of planar-grating diffraction. *J. Opt. Soc. Am.* **1981**, *71*, 811−818.
(46) Brundrett, D. L.; Glytsis, E. N.; Gaylord, T. K. Homogeneous layer models for high-spatial-frequency dielectric surface-relief gratings: conical diffraction and antireflection designs. *Appl. Opt.* **1994**, *33*, 2695−2706.

DOI: 10.1021/acsphotonics.8b00494
ACS Photonics 2018, 5, 3263−3271